





RESEARCH ARTICLE

Insights into molecular cluster materials with adamantane-like core structures by considering dimer interactions

Sebastian Schwan^{1,2} | Andreas J. Achazi^{1,2}  | Ferdinand Ziese^{2,3} |
Peter R. Schreiner^{2,4}  | Kerstin Volz⁵ | Stefanie Dehnen⁶ | Simone Sanna^{2,3}  |
Doreen Mollenhauer^{1,2} 

¹Institute of Physical Chemistry, Justus Liebig University, Giessen, Germany

²Center for Materials Research, Justus Liebig University, Giessen, Germany

³Institute of Theoretical Physics, Justus Liebig University, Giessen, Germany

⁴Institute of Organic Chemistry, Justus Liebig University, Giessen, Germany

⁵Department of Physics and Materials Science Center (WZMW), Philipps-Universität Marburg, Marburg, Germany

⁶Fachbereich Chemie, Philipps-Universität Marburg, Marburg, Germany

Correspondence

Doreen Mollenhauer, Institute of Physical Chemistry, Justus Liebig University, Heinrich-Buff-Ring 17, 35392 Giessen, Germany; Center for materials research, Justus Liebig University, Heinrich-Buff-Ring 16, 35392 Giessen, Germany.
Email: doreen.mollenhauer@phys.chemie.uni-giessen.de

Present address

Stefanie Dehnen, Institute of Nanotechnology, Karlsruhe Institut of Technology (KIT), Karlsruhe, Germany.

Funding information

Deutsche Forschungsgemeinschaft, Grant/Award Number: 398143140

Abstract

A class of adamantane-like molecular materials attracts attention because they exhibit an extreme non-linear optical response and emit a broad white-light spectrum after illumination with a continuous-wave infrared laser source. According to recent studies, not only the nature of the cluster molecules, but also the macroscopic structure of the materials determines their non-linear optical properties. Here we present a systematic study of cluster dimers of the compounds AdR_4 and $[(\text{RT})_4\text{S}_6]$ ($\text{T} = \text{Si}, \text{Ge}, \text{Sn}$) with $\text{R} = \text{methyl}, \text{phenyl}$ or 1-naphthyl to gain fundamental knowledge about the interactions in the materials. For all compounds, a similar type of dimer structures with a staggered arrangement of substituents was determined as the energetically most favorable configuration. The binding energy between the dimers, determined by including London dispersion interactions, increases with the size of the core and the substituents. The cluster interactions can be classified as substituent-substituent-dominated (small cores, large substituents) or core-core-dominated (large cores, small substituents). Among various possible dimer conformers, those with small core-core distances are energetically preferred. Trimer and tetramer clusters display similar trends regarding the minimal core-core distances and binding energies. The much lower energy barrier determined for the rotation of substituents as compared to the rotation of the cluster dimers past each other indicates that the rotation of substituents more easily leads to different conformers in the material. Thus, understanding the interaction of the cluster dimers allows an initial assessment of the interactions in the materials.

KEYWORDS

adamantane, amorphous molecular materials, cluster chemistry, DFT, theoretical concepts

1 | INTRODUCTION

Light-converting materials have become a key technology for reducing energy consumption in everyday illuminations and for devices such as

displays. Most prominent is the use of phosphors for white light-emitting diodes (LEDs).^{1–3} For example, the phosphors convert parts of the diode's blue light to a longer wavelength to produce white light. Recently, it was discovered that some materials consisting of

This is an open access article under the terms of the [Creative Commons Attribution-NonCommercial-NoDerivs](https://creativecommons.org/licenses/by-nc-nd/4.0/) License, which permits use and distribution in any medium, provided the original work is properly cited, the use is non-commercial and no modifications or adaptations are made.

© 2022 The Authors. *Journal of Computational Chemistry* published by Wiley Periodicals LLC.

organotetrel chalcogenide clusters with an adamantane-like core structure exhibit non-linear optical responses that enable the generation of highly directional white light when the material is illuminated by low-cost continuous-wave near-infrared laser diodes.^{4,5} Other materials exhibit this effect only when illuminated by intense, short-pulsed laser sources.^{6,7} This limitation, however, reduces the applicability of the conventional materials to only scientific and medical applications such as optical-coherence tomography or coherent anti-Stokes Raman-spectroscopy.^{6–11} Furthermore, materials for such applications often contain expensive rare-earth elements.¹² The new light-converting materials based on organotetrel chalcogenide clusters could therefore overcome these problems and replace current white-light emitters in high-brilliance applications.^{5,13}

The molecular materials of interest have adamantane-like core structures and organic substituents, usually with a cyclic π -electron system such as phenyl (Ph) or styryl (Sty) or without a π -electron system such as cyclohexyl (Cy).^{4,14–16} The adamantane-like core can be adamantane itself, giving AdR_4 (Ad = adamantane and R = organic substituent)^{15,17} or can be the inorganic $\{\text{T}_4\text{E}_6\}$ core of organotetrel chalcogenide compounds $[(\text{RT})_4\text{E}_6]$ (T = Si, Ge, Sn, E = S, Se, Te, and R = organic substituent).^{4,16,18–20} Depending on the composition of the cluster core and the nature of the organic substituents (and in some cases on the reaction conditions), the material can be amorphous or crystalline.¹⁴ However, when short-range order (e.g., because of π -stacking interactions) is present in these materials, or if the material is crystalline, the nonlinear white-light generation (WLG) is largely replaced by second-harmonic generation (SHG).^{15,16,21} In such cases, the frequency of the near-infrared laser is exactly doubled. Thus, it is assumed that for a cluster material to be a candidate for WLG, it must be amorphous. In an amorphous material, some short-range order may still be present, but the long-range order no longer exists.²² In order to understand and optimize the optical properties of this class of materials, it is therefore necessary to understand the geometric structures of the amorphous materials.^{23,24}

The first step towards understanding the geometric structures of the amorphous materials is to gain knowledge of the intermolecular interactions in the material. Therefore, in the present work, we obtain first insights into various amorphous cluster materials by investigating the interactions between the clusters in cluster dimers. Such small model systems have the advantage that *first principles* calculations can be applied for various cluster systems, which are computationally too demanding for the calculation of amorphous solid-state models. The focus of the investigation is on the cluster materials with cores of adamantane (Ad), $\{\text{Si}_4\text{S}_6\}$, $\{\text{Ge}_4\text{S}_6\}$, and $\{\text{Sn}_4\text{S}_6\}$, and substituents methyl (Me), phenyl (Ph), and 1-naphthyl (Np). This results in twelve clusters that differ in core structure, size, and polarizability. The substituents are either aromatic or aliphatic, and either small or relatively large (compared to the core structure). An investigation of this cluster series allows to identify fundamental similarities and differences as well as trends. Compared to our previous study on cluster dimers,¹⁸ this extended investigation covers many more chemical compositions, and thus allows for extended structural and energetic analyses.

The clusters with the $\{\text{Sn}_4\text{S}_6\}$ core have all been obtained and characterized experimentally. They represent amorphous materials, although the compound featuring Np substituents is found to show beginning order.^{4,18,21} The clusters with Ad or $\{\text{Ge}_4\text{S}_6\}$ cores have

been studied experimentally with Ph substituents.^{4,18,21} While crystalline and amorphous samples were prepared for 1,3,5,7-tetraphenyladamantane (AdPh_4), for $[(\text{PhGe})_4\text{S}_6]$ an amorphous material was obtained.^{4,15} The cluster compounds with $\{\text{Si}_4\text{S}_6\}$ core were obtained as crystalline compounds with Ph or Np substituents.^{4,18,21}

In the first step of this study, the geometric structures of the twelve cluster monomers and the energy barriers of the rotation of individual substituents were investigated. Next, the focus was on investigating the cluster dimers. For this purpose, extended tight-binding methods were used to support our density functional theory (DFT) calculations with dispersion corrections at B3LYP-D3(BJ)/cc-pVTZ//cc-pVDZ(-PP) level of theory. In this part of the study, we analyzed the minimum dimer structures regarding structural and energetic properties, before a large number of dimer conformers was analyzed against the background of possible structural units in amorphous materials. Furthermore, potential energy surfaces (PES) of cluster interactions and rotamerizations were generated to provide additional understanding of the diversity of the dimer conformers. For the dimer structures, exemplary density functional theory based calculations in the time domain reveal enhanced optical nonlinearities, in particular concerning the 3rd order optical susceptibility. Finally, cluster trimers and tetramers were looked at to better assess the applicability of the cluster dimer model system to extrapolate to interactions in larger systems.

1.1 | Computational details

To evaluate the equilibrium geometries of the single molecules and the dimer clusters, a three-step approach was employed. First, a conformational search was performed by utilizing the iterative metadynamics with genetic structure crossing (iMTD-GC) algorithm as implemented in the CREST program package.^{25,26} This was followed by structural optimizations using the extended tight-binding approach GFN2-xTB.^{27–29} Finally, the results were reoptimized with DFT at B3LYP-D3(BJ)/cc-pVDZ level of theory.

DFT calculations were performed using the Turbomole software package version 7.3.^{30,31} Structural optimization was carried out using B3LYP^{32–38} with an m4 grid³⁹ size and the resolution-of-identity (RI) approximation.⁴⁰ Test calculations using an m5 grid and no RI approximation led to negligible differences in the root mean squared displacement (RMSD <0.001 Å) and binding energies (<0.1% for m5 grid and <0.2% for RI). Medium- and long-range dispersion was accounted for by applying the D3 dispersion correction with Becke-Johnson damping by Grimme et al., which will be referred to as D3(BJ) in the following.^{41–43} Correlation consistent Dunning-type basis sets (cc-pVDZ and cc-pVTZ) were employed for all elements except Sn.^{44,45} For Sn, the energy-consistent scalar-relativistic effective core potential ECP28MDF was used in combination with the corresponding basis sets cc-pVDZ-PP and cc-pVTZ-PP,^{46,47} as received from Basis Set Exchange.^{48–50} Structural optimizations were carried out at the B3LYP-D3(BJ)/cc-pVDZ(-PP) level of theory, and single point calculations at B3LYP-D3(BJ)/cc-pVTZ(-PP) to calculate relative and binding energies. B3LYP-D3(BJ) is generally considered a reliable method, which was confirmed by our method assessment.^{51,52} The GFN2-xTB

method was used to calculate the potential energy surfaces and the minimum energy path was re-calculated at DFT level. The level of theory is based on a detailed method assessment regarding density functional, basis set and xTB that can be found in the Supporting Information Figures S1 and S2.

The structures were verified as the energetic minimum structures by numerical vibrational frequency calculations (electronic convergence: 10^{-7}). Frequency calculations using the cc-pVDZ(-PP) basis set result in no imaginary frequencies.

The energy barrier of the rotation of a single substituent on an optimized cluster monomer was calculated in 2° steps around the T–C bond (with T = C, Si, Ge, Sn) from 0° to 180° . Therefore, a constrained optimization was performed with the dihedral angle between the core and the substituent (along the T–C bond) fixed. All other parameters were freely relaxed. The relative energies of these optimized structures were used to determine the energy barrier of the rotation.

The binding energies ($E_{BE,dimer}$) were calculated as the difference of the total energies of the dimers and the monomers with the monomers in the geometric structure they have in the dimer, see Equation (1):

$$E_{BE,dimer} = E_{dimer} - E_{monomer1} - E_{monomer2} \quad (1)$$

Binding energies rather than dissociation energies were calculated because binding energies better represent molecule-molecule interactions in the solid state. The binding energy is equal to the difference of the dissociation energy ($E_{Diss,dimer}$ or D_e) and the deformation energy ($E_{Deform,monomers}$) of the monomers, see Equation (2):

$$E_{BE,dimer} = E_{Diss,dimer} - E_{Deform,monomers} \quad (2)$$

The binding energies of the dimers ($E_{BE,dimer}$) and the dissociation energies of the dimers ($E_{Diss,dimer}$) show the same general trends for the chemical systems presented (see Supporting Information Table S1). Considering the zero point vibrational energy (ZPVE) does not change this trend either ($E_{Diss,dimer}$ with ZPVE or D_0 , see Supporting Information Table S1).

The decomposition of the binding energies into different contributions was performed for the optimized cluster dimer structures. We also decomposed each cluster into its adamantane-like core and the substituents. The broken bonds of these substructures were saturated with hydrogen atoms. We then performed single point (SP) calculations for these fragments. Using the single point energy of each fragment, the decomposition of the binding energies were realized by subtracting the energy of the monomer fragments from the energy of the dimer fragment, as shown in Equations (3)–(5).

$$E_{BE,core-core} = E_{dimer\ cores} - E_{monomer1(core)} - E_{monomer2(core)}, \quad (3)$$

$$E_{BE,sub-sub} = E_{dimer\ sub} - E_{monomer1(sub)} - E_{monomer2(sub)}, \quad (4)$$

$$E_{BE,core-sub} = E_{BE,dimer} - E_{BE,core-core} - E_{BE,sub-sub}. \quad (5)$$

In addition to the decomposition into different structural parts, we performed an energy decomposition analysis (EDA) to

decompose the binding energies into the different energetic contributions: exchange-repulsion energy, orbital relaxation, dispersion interaction, electrostatic interaction, and correlation energy.^{53,54}

To obtain a complete overview about dimer conformers, a large number of dimer structures were created using the CREST program package^{25,26} in an energy window of 84 kJ mol^{-1} . The larger energy window leads to a variety of dimer cluster structures and thus a better representation of the conformational space, while excluding dimer conformations, which are energetically very unfavorable. The 20 lowest energy conformers for each chemical composition were selected and reoptimized at the B3LYP-D3(BJ)/cc-pVDZ(-PP) level of theory.

The potential energy surfaces (PES) were created by constrained-structure optimization calculations using the xTB software package utilizing the GFN2 algorithm.^{27–29} Constraints were set as force constants of $0.5\text{ Hartree Bohr}^{-2}$ applied to the coordinates of the core-atoms, excluding all hydrogen atoms of the organic adamantane compound. In total, 22,943 constrained optimizations were performed for each structure (PES A: 9821, PES B: 6561, PES C: 6561). The energy of each structure was calculated with single-point calculation at B3LYP-D3(BJ)/cc-pVTZ(-PP) level of theory.

The calculation of the nonlinear optical response of single molecules and dimers was performed by DFT within the supercell approach. The software packages Quantum Espresso^{55,56} and Yambo⁵⁷ were therefore employed. PAW potentials⁵⁸ including $2s^2$ and $2p^2$ electrons for C and the $1s$ electron for H, respectively, describe the electron-ion interaction. We adopted the PBE formulation^{59,60} of the generalized gradient approximation⁶¹ for the exchange and correlation functional, which has proven in the past to correctly describe the clusters.¹⁴ Plane waves up to a cutoff of 56 Ry were used as basis for the expansion of electron wave functions, while the energy integration of the Brillouin zone is performed on a $2 \times 2 \times 2$ Monkhorst-Pack⁶² k-point mesh. The molecular clusters are modeled within a box of $5 \times 10^4\text{ \AA}^3$. The atomic positions were relaxed until the residual Hellmann-Feynman forces⁶² are lower than 0.005 eV/\AA , whereby van der Waals interactions were accounted for by a semi-empirical DFT-D3 scheme with zero damping.^{41,63}

The nonlinear optical susceptibilities of second and third order $\chi^{(2)}$ and $\chi^{(3)}$ were calculated within the independent particle approximation in the time-domain by developing the dynamical polarization (calculated within the Berry-phase⁶⁴ formulation) in a power series of the applied field.^{65,66} Thereby 252 electronic bands were considered for isolated cluster and 504 for cluster dimers. The nonlinear optical coefficients of isolated molecules and dimers were obtained by averaging the cartesian components of the hyperpolarizability tensor.

The calculation of larger systems, namely cluster trimers and tetramers, followed the same three-step procedure used for the monomer and dimer structures. The structures resulting from these optimizations were then used to calculate the total binding energies

per molecule. Here, the total binding energies were calculated, divided by the number of clusters or molecules in the system and compared to the corresponding systems of different sizes. For the total binding energies, we used the following formulas to calculate the average binding energy per cluster:

$$E_{BE,dimer} = (E_{dimer} - E_{monomer1} - E_{monomer2})/2, \quad (6)$$

$$E_{BE,trimer} = (E_{trimer} - E_{monomer1} - E_{monomer2} - E_{monomer3})/3, \quad (7)$$

$$E_{BE,tetramer} = (E_{tetramer} - E_{monomer1} - E_{monomer2} - E_{monomer3} - E_{monomer4})/4. \quad (8)$$

TABLE 1 Rotational barriers for the rotation of a single substituent at the cluster around the respective T–C bond, calculated at the B3LYP-D3(BJ)/cc-pVTZ(-PP)//cc-pVDZ(-PP) level of theory. Also, the core-volume, calculated via a convex hull around the core atoms, excluding hydrogen, is shown.

Compound	Rotational barrier (kJ mol ⁻¹)	Core volume (Å ³)
AdMe ₄	15	9.3
[(MeSi) ₄ S ₆]	5	26.7
[(MeGe) ₄ S ₆]	3	29.9
[(MeSn) ₄ S ₆]	1	38.0
AdPh ₄	4	9.4
[(PhSi) ₄ S ₆]	1	26.6
[(PhGe) ₄ S ₆]	1	29.8
[(PhSn) ₄ S ₆]	1	37.9
AdNp ₄	27	9.4
[(NpSi) ₄ S ₆]	16	26.6
[(NpGe) ₄ S ₆]	13	29.8
[(NpSn) ₄ S ₆]	9	37.9

2 | RESULTS AND DISCUSSION

2.1 | Geometric structures and rotational barriers of the single cluster

Considering single clusters is the first step in understanding the structural flexibility within the dimer systems. Since the cluster core architectures and the organic structures of the substituents are relatively rigid, the conformational changes regarding the rotation of the substituents need to be considered. Thus, for each cluster, a number of different conformers can be determined depending on the rotation of each substituent, for example, 81 conformers were found within 7 kJ mol⁻¹ for AdPh₄. Starting with the determined global minimum structures according to the three-step procedure, the rotational barriers are shown in Table 1. The global minimum structures are shown in Figure 1 for the examples AdPh₄, [(NpSi)₄S₆], and [(MeSn)₄S₆], all other structures can be found in Figure S3.

Table 1 shows that cluster monomers with a larger volume of the core structure, as calculated via a convex hull around the core atoms, excluding hydrogen [Ad (9 Å³) < {Si₄S₆} (27 Å³) < {Ge₄S₆} (30 Å³) < {Sn₄S₆} (38 Å³)] possess lower rotational barriers for the substituents. This can be explained by the increasing T–C distance between the core and the substituent from 1.53 Å (C–C) to 1.87 Å (Si–C) and 1.95 Å (Ge–C) to 2.14 Å (Sn–C). This increasing distance leads to a decrease in steric hindrance. Hyperconjugation also plays an important role in the stabilization of the conformers, especially in the organic compounds. This additional stabilization by hyperconjugation in the organic compounds leads to much larger rotational barriers for the organic compounds. The Ad core structure exhibits particularly large rotational energy barriers due to the additional hydrogen atoms of the CH₂ bridges. This is especially strong for the naphthyl-substituted structures.

The results indicate negligibly small rotational barriers for all inorganic compounds with Me substituents and all compounds with Ph



FIGURE 1 Minimum structures of cluster monomers optimized at B3LYP-D3(BJ)/cc-pVDZ(-PP) level of theory. Left: AdPh₄, middle: [(NpSi)₄S₆], right: [(MeSn)₄S₆]. Color code: gray: carbon, white: hydrogen, yellow: sulfur, brown: silicon, blue: tin

substituents. Their barriers are close to the thermal energy at room temperature, which means that we can expect free rotation at room temperature and that all energy levels should be significantly occupied. Since energetic barriers of up to ~ 100 kJ mol⁻¹ are surmountable for the other cluster compounds at room temperature,⁶⁸ all substituents of all core structures are able to rotate.

2.2 | Analysis of the global minimum dimer structures

The global minimum structures for each cluster dimer were analyzed regarding fundamental structural parameters and total binding

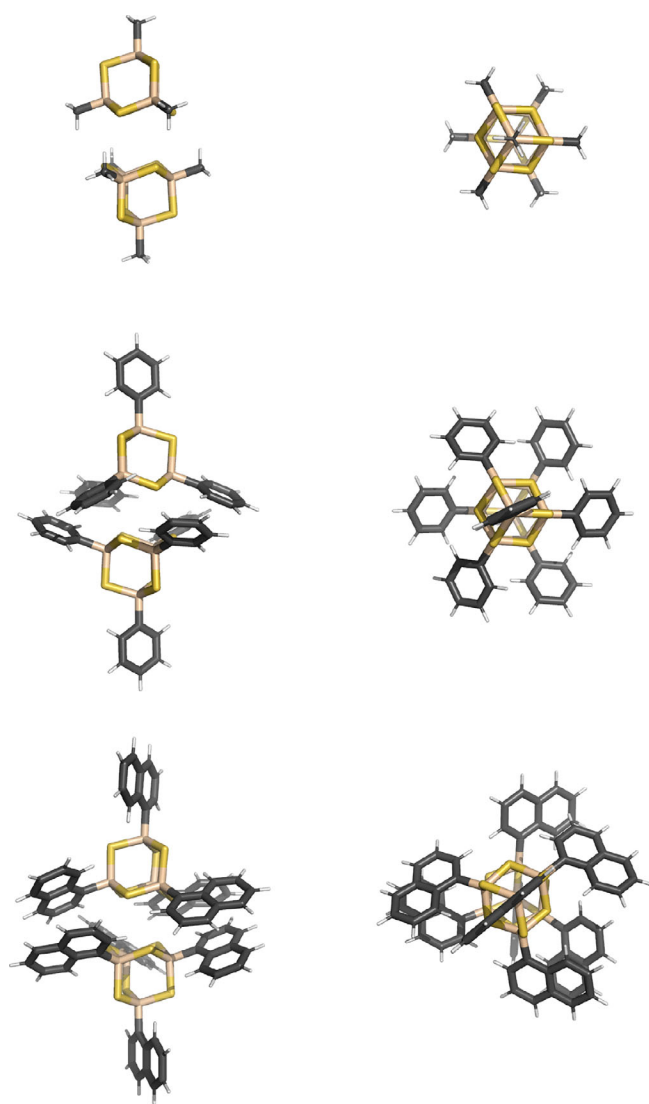


FIGURE 2 Lowest energy structures of [(RSi)₄S₆] (R = Me, Ph, Np) created using with the iMTD-GC algorithm with subsequent optimization at GFN2-xTB and then at B3LYP-D3(BJ)/cc-pVDZ(-PP) level of theory. Left: View perpendicular to core–core axis, right: view along core–core axis. Color code: gray: carbon, white: hydrogen, yellow: sulfur, brown: silicon

energies. In Figure 2, the optimized structures of the {Si₄S₆}-based systems are shown as an example. All other optimized minimum structures are shown in Figure S4.

The minimum structures for the Me- and Ph-substituted dimers are very similar regarding the core and substituent orientation. Three out of the four substituents of each cluster have a direct interaction with the other cluster. In all cases, the two clusters are orientated such that the three substituents of one cluster are located in the three gaps between the substituents of the other cluster. These types of dimers are referred to as ‘staggered’ dimers. While for AdNp₄, [(NpSi)₄S₆], and [(NpGe)₄S₆], almost staggered but slightly rotated dimers are present, for [(NpSn)₄S₆], the naphthyl substituents are located flat on top of each other (eclipsed). We assume that steric interaction and the medium- and long-range dispersive interactions are responsible for these structures to preferably form staggered configurations.

The core–core distances shown in Table 2 increase almost linearly with the core volume, with the exception of [(MeSn)₄S₆], which has a slightly smaller core–core distance than [(MeSi)₄S₆] and [(MeGe)₄S₆]. The Ph-substituted clusters have a smaller core–core distance than the Me substituted ones. This is most likely due to the stronger Ph–Ph interactions. These interactions are mainly dispersive and show C–H- π interactions. Overall, this leads to higher binding energies in the dimers. The only exception in this comparison is the Sn-based clusters, where the core–core distances are very similar. In contrast, the Np-substituted clusters have larger core–core distances than the Ph-substituted ones due to larger steric hindrance, although the dispersion interactions and thus the binding energies are larger than for Me- and Ph-substituted cluster.

Table 2 shows that the total binding energy increases from the small Me substituent (average binding energy for all compounds: -63 kJ mol⁻¹) to the medium sized Ph substituent (average binding energy for all compounds: -138 kJ mol⁻¹) to the largest Np substituent (average binding energy for all compounds: -174 kJ mol⁻¹).

TABLE 2 Core–core distances and the binding energies in dimers of the different compounds calculated at the B3LYP-D3(BJ)/cc-pVTZ (-PP)//cc-pVDZ(-PP) level of theory

Compound	Core–core distance (Å)	$E_{BE,dimer}$ (kJ mol ⁻¹)
AdMe ₄	6.16	-22
[(MeSi) ₄ S ₆]	6.21	-62
[(MeGe) ₄ S ₆]	6.24	-68
[(MeSn) ₄ S ₆]	6.18	-101
AdPh ₄	5.89	-117
[(PhSi) ₄ S ₆]	6.02	-136
[(PhGe) ₄ S ₆]	6.07	-140
[(PhSn) ₄ S ₆]	6.17	-160
AdNp ₄	5.97	-152
[(NpSi) ₄ S ₆]	6.19	-169
[(NpGe) ₄ S ₆]	6.42	-178
[(NpSn) ₄ S ₆]	6.80	-200

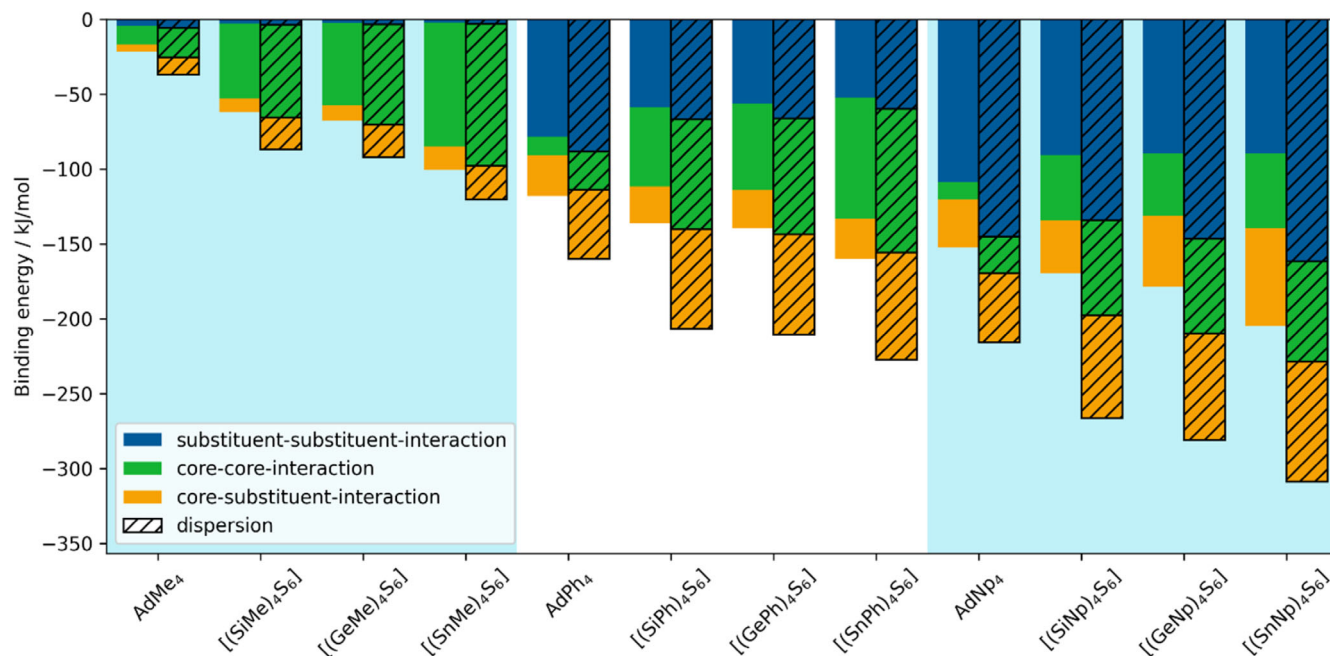


FIGURE 3 Decomposition of the binding energy contributions of the global minimum cluster dimers into substituent-substituent, core-core, and substituent-core interactions calculated at the B3LYP-D3(BJ)/cc-pVTZ(-PP)/cc-pVDZ(-PP) level of theory. The hashed bars represent only the dispersive energy contributions (estimated by the dispersion correction), while the unhashed bars represents the total binding energy contributions

2.3 | Decomposition of binding energies of the global minimum structures

The energy decomposition analysis (EDA) for the dimer systems (Figure S5) indicates that the largest contribution to the binding energy comes from the medium to long-range dispersion interactions. Other contributions such as orbital relaxation, electrostatic interactions, and electron correlation interactions scale almost linearly with the total binding energies in the dimers along the different chemical compositions, leading to insignificant systematic differences between the various chemical systems apart from scaling with the total binding energy. The only repulsive energy contribution is the Pauli exchange-repulsion energy (Figure S5). The dispersion energy can be well estimated by the dispersion correction and also represents the energy contribution,⁶⁷ which can be best modified by changing the materials (core structure and substituents). Therefore, only the total energy and the dispersion energy contributions are distinguished in the following.

Figure 3 represents the medium-to-long-range dispersion interactions (estimated by the dispersion correction, hashed bars) as the dominant factor to the binding energies of dimers. Without this dispersion energy, the binding energy contributions are not sufficient for a binding interaction. This is also to be expected since there are no hydrogen bonds or significant permanent dipoles present in the clusters that could exceed the dispersion energies.

In the next step, the binding energies of the dimers were structurally decomposed into the core-core, substituent-substituent, and core-substituent interactions as done in Reference 18 (Figure 3). The core-core dimer interactions increase from the smallest core structure

(adamantane) through the medium-sized cores ($\{Si_4S_6\}$ and $\{Ge_4S_6\}$) to the largest core structure ($\{Sn_4S_6\}$). The differences are significant. The core-core interaction for $[(RS)_4S_6]$ with $R = Me$ or Ph is about six to seven times stronger than for the corresponding adamantane-based clusters, and about 50% stronger than in the Si- and Ge-based compounds. For the naphthyl compounds, these differences turn out to be smaller because of the larger core-core distances.

Furthermore, the substituent-substituent interactions decrease from adamantane-based structures through the $\{Si_4S_6\}$ - and $\{Ge_4S_6\}$ -based structures to the $\{Sn_4S_6\}$ -based core structure. This trend is particularly evident in the Ph-substituted compounds (Figure 3). This decrease can be simply explained by the increasing size of the core structures, which leads to larger distances between the substituents of the different clusters (Table 2). The substituent-substituent interactions also increase with the substituent size ($Me < Ph < Np$) due to increased dispersion interactions. The steric hindrance for the Np-substituted compounds leads to a larger core-core distance (Table 2), which in turn reduces the core-core interactions. The increase of the core-substituent interactions for larger core sizes and larger substituents can also be explained by the increasing dispersion interactions.

The results show that the ratio of the substituent-substituent interactions to the core-core interactions varies systematically for the different chemical compositions. This leads to dimer interactions, which are more likely to be caused by core-core interactions or substituent-substituent interactions. This distinction could possibly serve as a rough indicator which type of (dis)order to be realized in the material. The isotropic core-core interactions could thereby rather

be associated with a tendency for lower order in the material. For example, this approach was successful in comparing $[(\text{NpSn}/\text{PhSn})_4\text{S}_6]$ and the $\{\text{Si}_4\text{S}_6\}$ -based homologs.¹⁸ In the case of $[(\text{NpSn})_4\text{S}_6]$, in the cluster dimers, the binding contribution of the interaction of the substituents is about equal to the binding energy contribution of the interaction of the cores. Consequently, a macroscopic structure with a crystalline or amorphous nature could be possible. This is in agreement with the scanning precession electron diffraction data of the material that show a mixture of amorphous and crystalline regions (see supporting information Figure S5). However, as soon as the differences in the macroscopic material (as for Si or Ge) or the reaction conditions (as in AdPh_4) play a major role, such conclusions are less obvious.^{4,15,18}

2.4 | Analysis of different dimer conformers

Since some of the investigated clusters form amorphous solids, it can be assumed that several different cluster dimer conformers are present in the real solid materials. The conformer search yielded widely varying dimer conformers, which differ in the relative orientation of the two clusters. Figure 4 shows some example structures of $[(\text{PhSi})_4\text{S}_6]_2$. The different structures can be roughly classified by the number of substituent contacts between one cluster and the other or the structure type. From this, four main categories of dimer conformers can be derived: “staggered,” “eclipsed,” “shifted,” and “single-substituent-contact.”

The maximum possible number of contacts between substituents is illustrated in Figure 4 by the lowest energy dimer with **4a** a staggered structure and **4b** an eclipsed structure. In these, three substituents of one cluster are in direct contact with three substituents (3–3) of the other cluster, resulting in small core–core distances and strong binding energies (Figure 4). The structures shown in Figure 4c, d are 2–2 contact structures. This results in larger core–core distances and weaker binding energies, as compared to the 3–3 contact structures. Figure 4f shows a 1–1 contact structure. Other configurations and transitions of these conformers (e.g., 3–2 and 3–1) are also possible.

The core–core distances of the various dimer conformers are smallest for the lowest energetic minimum structures. The dimer conformers of the different compositions “staggered,” “eclipsed,” “shifted,” “single-substituent-contact” show similar pattern in the core–core distances. The first gap in the core–core distances appears in the range between 6.5 and 8 Å. This gap separates the staggered and eclipsed minimum conformers from the shifted ones (see Figure 5 for examples). A second, larger gap appears in the range between 8 and 11 Å. At these large core–core distances, one finds only structures with 1–1 contact. The compounds dominated by core–core interactions, $[(\text{MeGe})_4\text{S}_6]$ and $[(\text{RSn})_4\text{S}_6]$ ($\text{R} = \text{Me}, \text{Ph}, \text{Np}$), do not exhibit 1–1 contact structures in the observed energetic region (84 kJ mol^{-1} above the energetic minimum). This can be explained by the larger core–core distance in the 1–1 structures, which would lead to much lower binding energies for these systems.

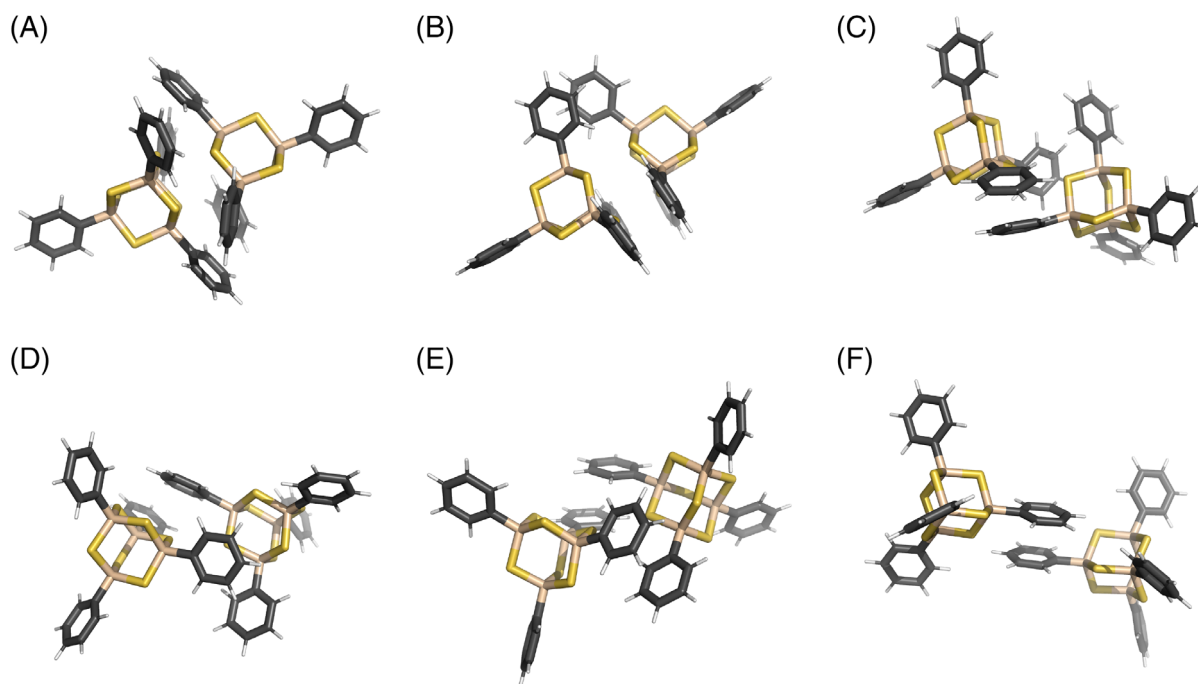


FIGURE 4 Example structures with different core–core distances, obtained with CREST, subsequently optimized using B3LYP-D3(BJ)/cc-pVDZ(-PP). (a) Core–core distance: 6.02 Å (staggered, 3–3), (b) core–core distance: 6.49 Å (eclipsed, 3–3), (c) core–core distance: 8.13 Å (shifted, 2–2), (d) core–core distance: 8.21 Å (shifted, 2–2), (e) core–core distance: 8.29 Å (shifted, 2–2), (f) core–core distance: 11.14 Å (1–1). Color code: gray: carbon, white: hydrogen, yellow: sulfur, brown: silicon

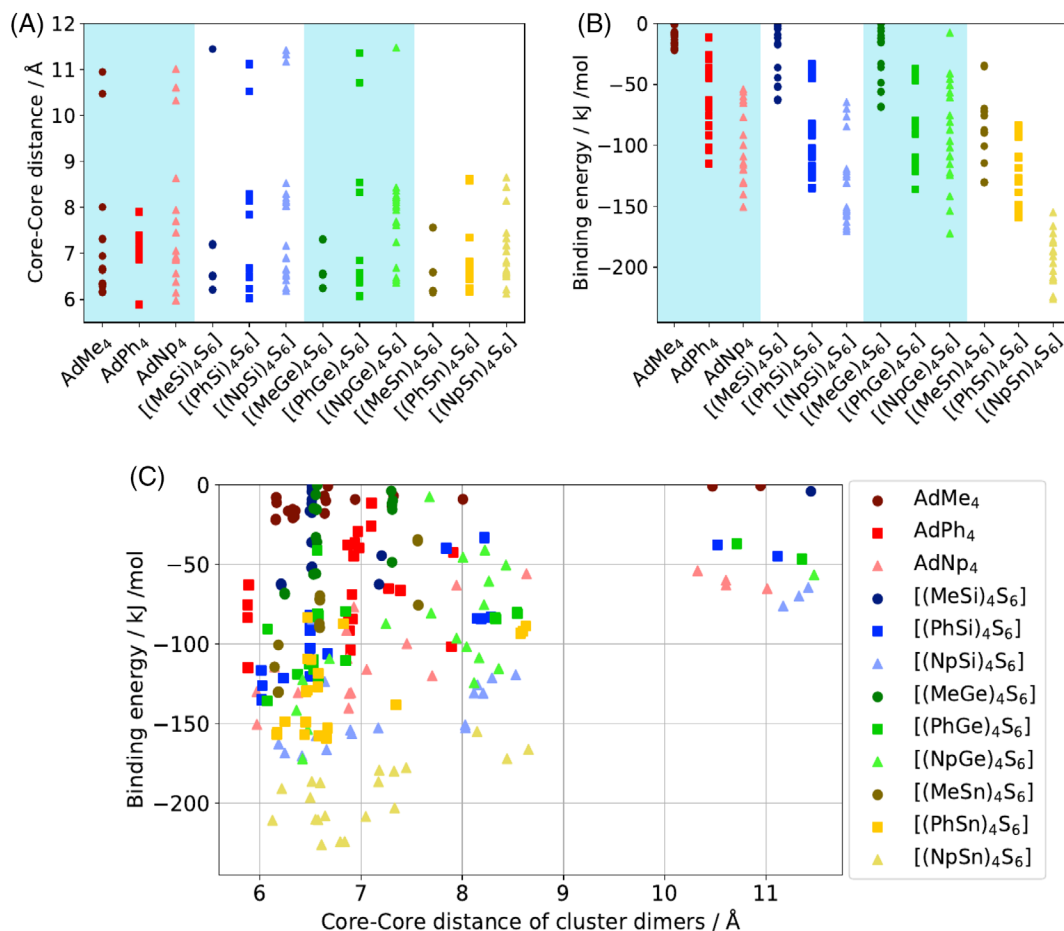


FIGURE 5 Results of DFT-based analysis of the structures from CREST conformational analysis. (a) Core–core distances of the optimized dimer structures, (b) binding energies for dimer structures, and (c) scatter plot of the core–core distances (x-axis) versus the binding energies (y-axis)

The binding energies shown in Figure 5b follow the overall trend of the core–core distances. The minimum structures again form the lower bound. It is notable that the gaps separating the staggered/eclipsed structures, the shifted structures and the 1–1 contact structures are also present. Figure 5c shows that the core–core distances and the binding energies are correlated.

2.5 | Calculation on the nonlinear optical response

The effect of the cluster–cluster interaction on the nonlinear optical response of the cluster structures was investigated using AdPh₄ as a model system. Figures 6 and 7 (light blue curves) show the optical susceptibilities of the 2nd and 3rd order, respectively, calculated for isolated AdPh₄ clusters. The $\chi^{(2)}$ spectra show the classic peak above 2 eV, typical of clusters featuring phenyl rings¹⁴ and originating by electronic transitions within the delocalized orbitals of the substituents. The $\chi^{(3)}$ spectrum is dominated by a peak at about 1.6 eV which is roughly 1/3 of the fundamental HOMO–LUMO transition.

To investigate the effect of the dimer formation on the optical response, we calculated the nonlinear optical coefficients of AdPh₄

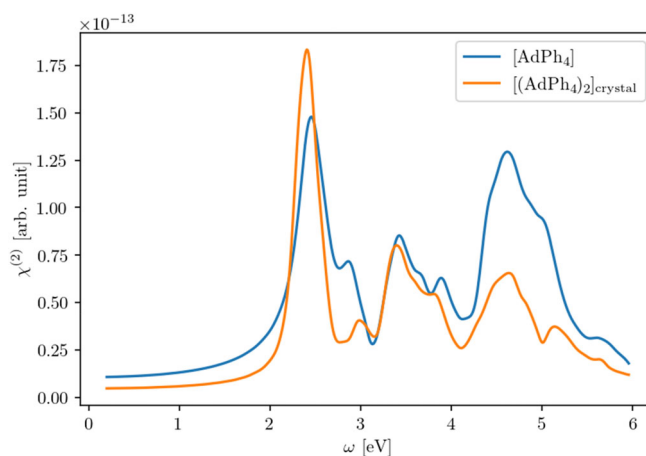


FIGURE 6 Second order susceptibility $\chi^{(2)}$ calculated within the independent particle approximation in the time-domain approach for AdPh₄ isolated clusters (light blue line) and AdPh₄ cluster dimers in the nearest neighbors geometry of AdPh₄ crystals (orange line)

cluster dimers. We thereby employ the structure of the nearest neighbor dimers in AdPh₄ crystals. The results are shown in Figures 6 and 7 (orange curves). The 2nd order optical susceptibility is not drastically

modified upon dimer formation. However, the intensity of the main peak is enhanced, while the nonlinearities for lower photon energies are slightly reduced. Concerning the 3rd order optical coefficients, an overall strong enhancement of the optical response is predicted.

2.6 | Potential energy surfaces of cluster-cluster interactions

To gain insights about the energy barriers and conformers close to the preferred staggered and eclipsed cluster dimer structures, potential energy surfaces (PESs) were created using the semiempirical GFN2-xTB-algorithm starting from an idealized structure. The substituents of the idealized starting structures are aligned in a plane to ensure a low repulsive interaction of the substituents during rotation. Note that the energetic differences between the global minimum dimers and the idealized structure determined by the PES are very

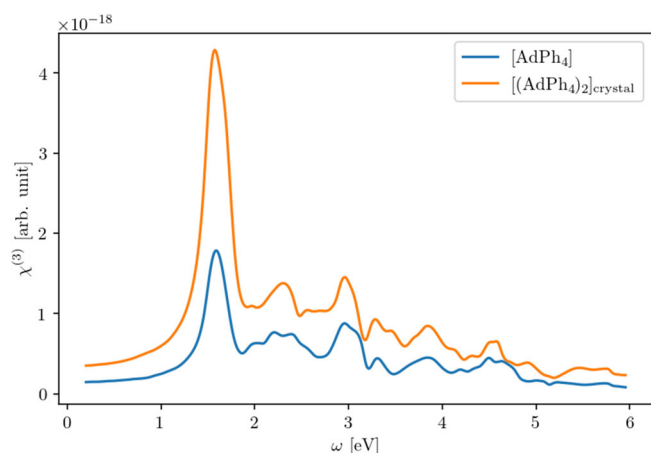


FIGURE 7 Third order susceptibility $\chi^{(3)}$ calculated within the independent particle approximation in the time-domain approach for AdPh_4 isolated clusters (light blue line) and AdPh_4 cluster dimers in the nearest neighbors geometry of AdPh_4 crystals (orange line)

small (about 2.5 kJ mol^{-1} on average). Moreover, both of the structures are staggered and very similar to each other.

The first PES (PES A) represents a variation of the core–core distance with a concomitant change of the relative rotation of the monomers to each other. PESs A of the $\{\text{Si}_4\text{S}_6\}$ -based compounds are shown in Figure 8 as an example; those of the other compounds are provided in the supporting information (Figure S6). For each angle of rotation, an energy minimum at the PES was determined, which is associated with a specific core–core distance. These minimum values are highlighted in red in Figure 8 and Figure S6 and represent the minimum path along the performed rotation. From this minimum energy path, the rotational energy barrier and the rotational distance were determined (Figure 9). The rotational energy barrier represents the energy difference between the highest and lowest energy of the path. The rotational distance is the difference between the largest and smallest core–core distance. The results of these calculations are listed in Table 3.

The general trend of the rotation barriers is consistent for GFN2-xTB and B3LYP-D3(BJ) calculations, with the exception of $[(\text{NpSn})_4\text{S}_6]$. For cluster dimers with the smaller Me and Ph substituents, the rotation barrier increases with increasing size of the core volume. The naphthyl substituents show the opposite trend. Structures with $[(\text{RSi})_4\text{S}_6]$ and $[(\text{RGe})_4\text{S}_6]$ cores generally exhibit very similar rotation barriers.

Our results indicate a relatively high mobility for AdMe_4 molecules in terms of rotation towards other AdMe_4 molecules. All other systems will be mainly found close to their global minimum structure. Comparison of the dimer rotational barrier with the rotation of a single substituent (see Table 1) reveals for the latter values that are by about one order of magnitude smaller with the exception of the value computed for AdMe_4 . It can be concluded that the orientation of two clusters relative to each other generally has a much greater impact on the energetic landscape of the material than the orientation of the substituents at each individual cluster. Thus, it can be assumed that the rotation around the substituents may also lead to different conformers in the material more easily than the dimer rotation.

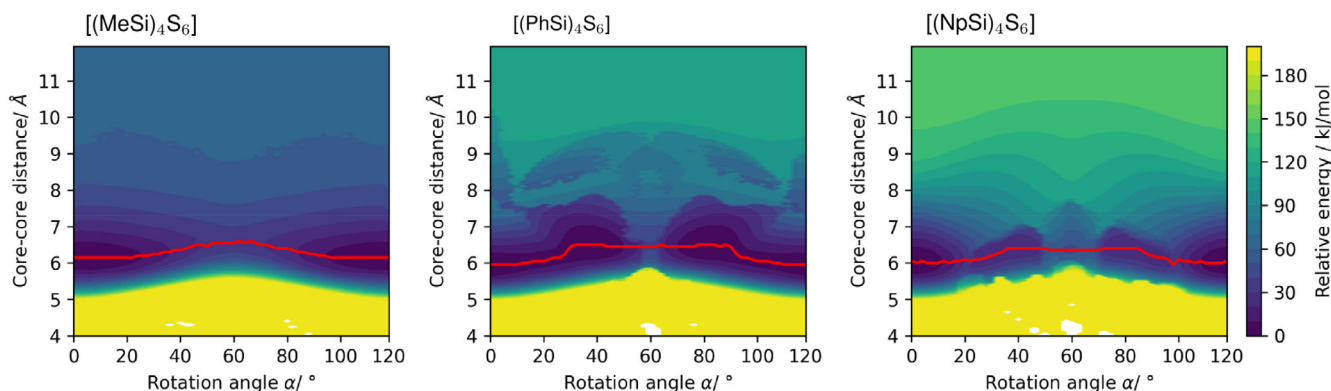


FIGURE 8 Potential energy surfaces A as a function of the distance between the clusters and the relative rotation angle of $[(\text{RSi})_4\text{S}_6]$ [R = Methyl (left), phenyl (middle) or naphthyl (right)] calculated by a constrained optimization at the GFN2-xTB level of theory

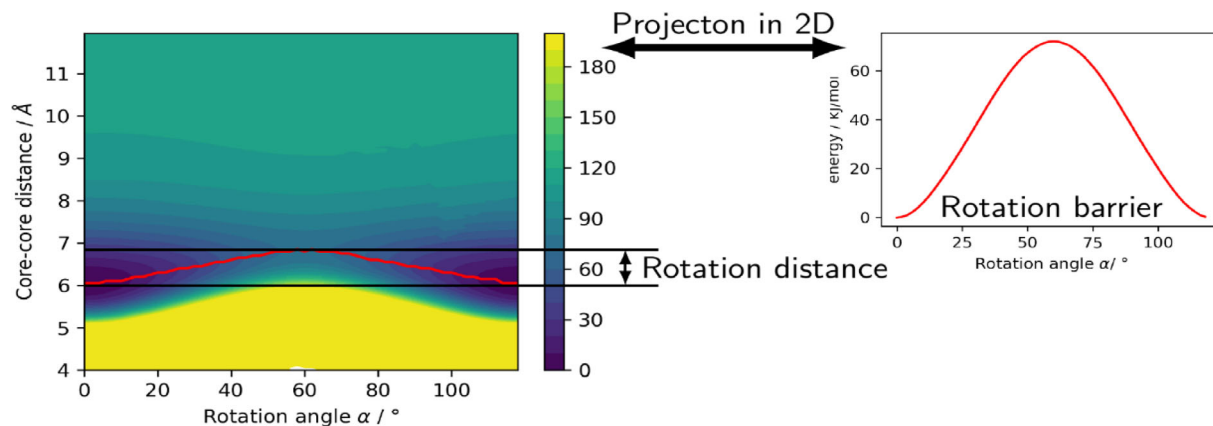


FIGURE 9 Visual representation of the energetic rotation barrier and rotation distance extracted from the potential energy surfaces. The red line shows the minimum energy path for the rotation

Cluster	Rotational distance (GFN2-xTB) (Å)	Rotational barrier (GFN2-xTB) (kJ mol ⁻¹)	Rotational barrier (B3LYP-D3(BJ)/cc-pVTZ(-PP)) (kJ mol ⁻¹)
AdMe ₄	0.30	4	5
[(MeSi) ₄ S ₆]	0.45	35	62
[(MeGe) ₄ S ₆]	0.65	39	55
[(MeSn) ₄ S ₆]	0.80	72	69
AdPh ₄	1.00	20	49
[(PhSi) ₄ S ₆]	0.55	39	83
[(PhGe) ₄ S ₆]	0.65	48	87
[(PhSn) ₄ S ₆]	0.85	82	101
AdNp ₄	2.15	87	135
[(NpSi) ₄ S ₆]	0.45	53	111
[(NpGe) ₄ S ₆]	0.55	49	99
[(NpSn) ₄ S ₆]	0.80	62	84

TABLE 3 Rotational distances and rotational barriers of the total energies determined with the PES A calculated at GFN2-xTB and B3LYP-D3(BJ)/cc-pVTZ(-PP) level of theory are given

In agreement with the global minimum search, the energetically lowest structure is a staggered arrangement with a rotation angle of 0° (Figures 8 and 9). This cluster dimer is indistinguishable from its conformers with a rotation angle of 120° and 240° due to symmetry. The structure with the highest energy on the minimum energy path for the rotation exhibits a rotation angle of 60° and is a eclipsed structure with the substituents directly aligned. The eclipsed structures have larger core–core distances than the staggered ones due to the stronger steric repulsion of the substituents (Figure S7).

The second and third PESs (PES B and PES C) represent a variation of the displacement of one cluster on a plane perpendicular to the core–core axis of the two clusters, with a fixed rotation angle and a fixed height in the direction of the core–core axis. The PESs are calculated with a staggered conformation (0° rotation angle) and with eclipsed conformation (60° rotation angle), see Figure 10 for the [(PhSi)₄S₆] structure. These two PESs differ in the relative rotation of the cluster, leading to different minima on the PESs and different symmetry. The PESs of the dimers with other chemical compositions are shown in Figures S8 and S9.

The alternating, low energy cluster dimer (Figure 10, left) forms a PES with approximately *D*_{3h} symmetry. The minimum is located exactly in the center of the PES, and it is consistent with the global minimum structure found using the iMTD-GC algorithm (Figure S4). For the eclipsed high-energy dimer (Figure 10, right), a PES with an approximate *C*₆ point group ensues. The lowest-energy structure is located in a circular region around the center of the PES. The observed location of the energetic minimum suggests that, in an eclipsed structure, the relative orientation of the cluster shifts from directly aligned molecules to slightly shifted molecules in order to reduce the repulsion energy in the system, making the existence of a mirror plane (perpendicular to the bond axis) energetically unfavorable for this orientation.

Consequently, the global minimum for the energetically preferred staggered dimer structure is a conformer with inversion symmetry, while the eclipsed structure has no inversion center. This could be a crucial point for the nonlinear optical properties of large solid-state structures, since inversion symmetry in the crystal structures is known to prevent the here unwanted SHG—at least in perfect single crystals.⁵

FIGURE 10 Potential energy surfaces B and C with respect to a displacement of the clusters on a hyperplane perpendicular to the bond axis of the $[(\text{PhSi})_4\text{S}_6]$ compound. The PESs were calculated for two different relative rotation angles: 0° (staggered, left) and 60° (eclipsed, right). These PESs were created using constrained optimization calculations on the GFN2-xTB³⁴ level of theory. Color code: gray: carbon, white: hydrogen, yellow: sulfur, brown: silicon

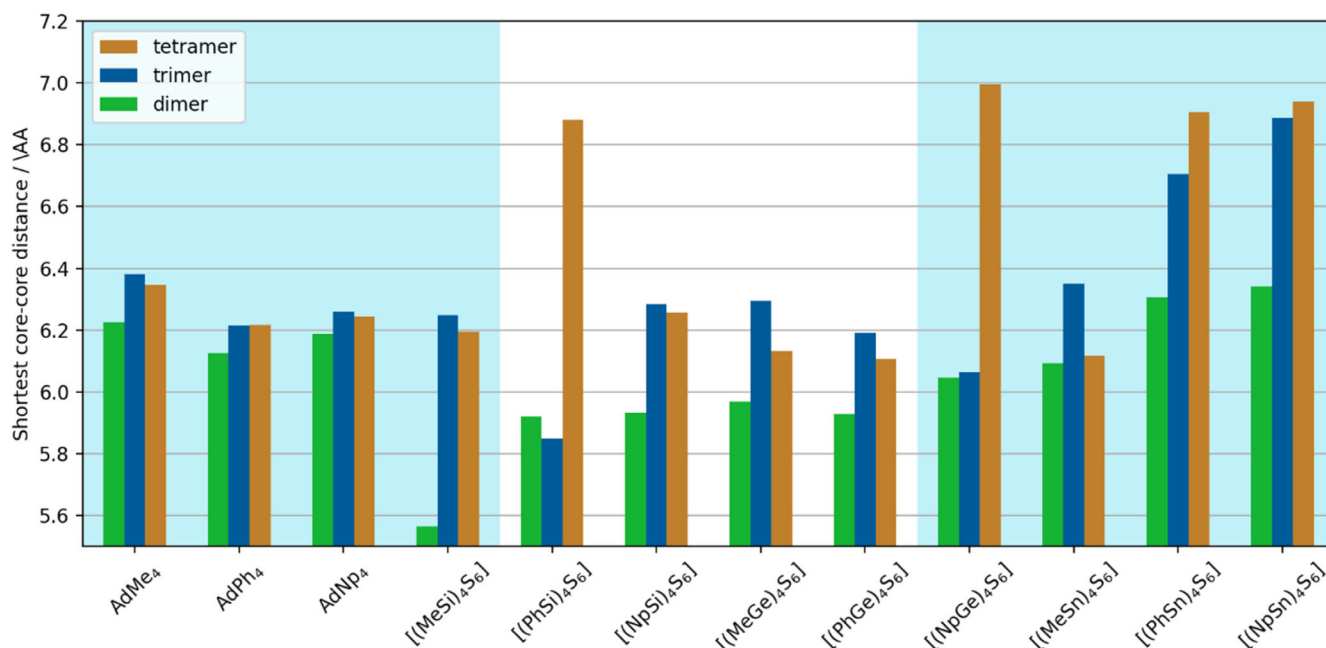
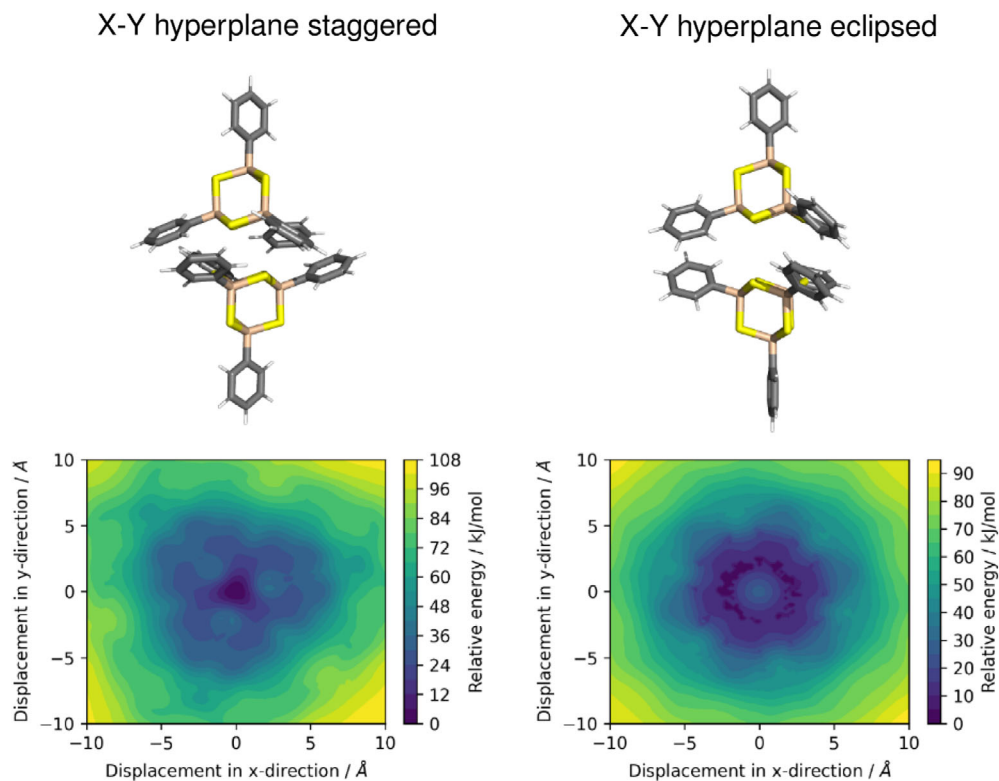


FIGURE 11 Comparison of the core-core distances of the trimer and tetramer structures with the core-core distance of the corresponding dimer structure. For all structures, the energetic minimum structure was obtained by CREST, which was subsequently optimized at B3LYP-D3 (BJ)/cc-pVDZ(-PP) level of theory

2.7 | Extension to trimer and tetramer cluster systems

The analysis of cluster dimers is now extended to larger systems with three clusters (trimer) and four clusters (tetramer). The

resulting minimum structures of the trimers are shown in Figure S10 and the structures of the tetramers are shown in Figure S11. The trimers and tetramers were studied to estimate the transferability and scaling of the conclusions of small dimer systems to larger agglomerates. For this purpose, we have mainly

considered the core–core distances and the binding energies as structural and energetic descriptors.

To make the core–core distances of the trimer and tetramer structures comparable to those of the dimer structures, we analyzed the smallest core–core distance within the trimer and tetramer structure and compare it to the core–core distance of the obtained minimum dimer structure. Figure 11 shows that the core–core distance varies up to 1 Å for $[(\text{MeSn})_4\text{S}_6]$, AdPh_4 and AdNp_4 while yielding very good agreement (within 0.3 Å) for all other structures.

Different dimer configurations lead to different core–core distances. The energetically preferred relative orientation of two clusters can change when more clusters are added to the system. For example, an exact representation of the energetically preferred staggered dimer structure cannot be found for most trimer or tetramer structures,

which leads to larger core–core distances of dimers in these agglomerates. This is also demonstrated in the overlay of the minimum structures (Figures 12 and S12) of the preferred dimers, trimer, and tetramer agglomerates. In the larger agglomerates, we see a wide variety of all different types of cluster–cluster interaction (3–3, 2–2, 3–2, 1–1, 2–1, and 3–1). Thus, to represent the cluster–cluster interaction of a large extended system, the consideration of multiple dimer conformers seems reasonable.

For the binding energies of the different chemical compositions across the different system sizes, Figure 13 shows that the trends of the dimers with respect to the core type (increasing from Ad over $\{\text{Si}_4\text{S}_6\}$ and $\{\text{Ge}_4\text{S}_6\}$ to $\{\text{Sn}_4\text{S}_6\}$) and substituents (increasing from Me over Ph to Np) are consistent with that found for the trimers and tetramers. Note that the average binding energy per molecule increases

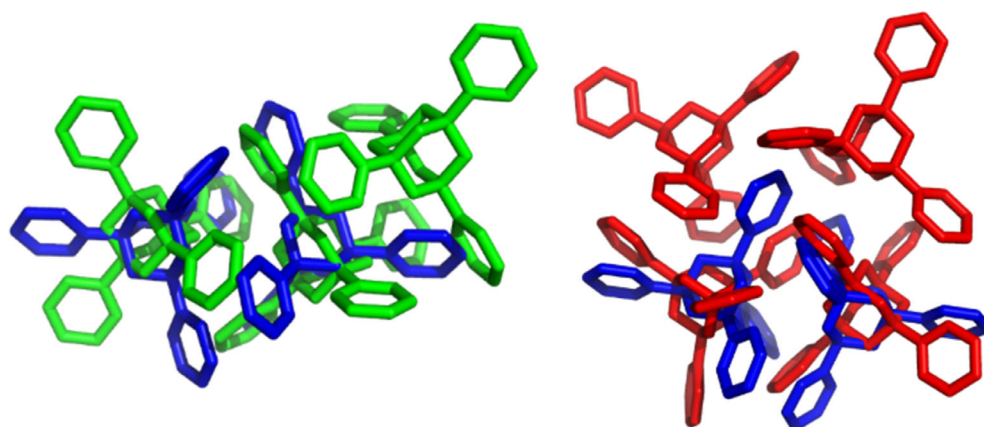


FIGURE 12 Overlay of the energetically preferred dimer structure (blue) of AdPh_4 with the corresponding energetically preferred trimer (green) and tetramer structure (red). For all structures, the energetic minimum structure was obtained by CREST, which was subsequently optimized at B3LYP-D3(BJ)/cc-pVDZ(-PP) level of theory

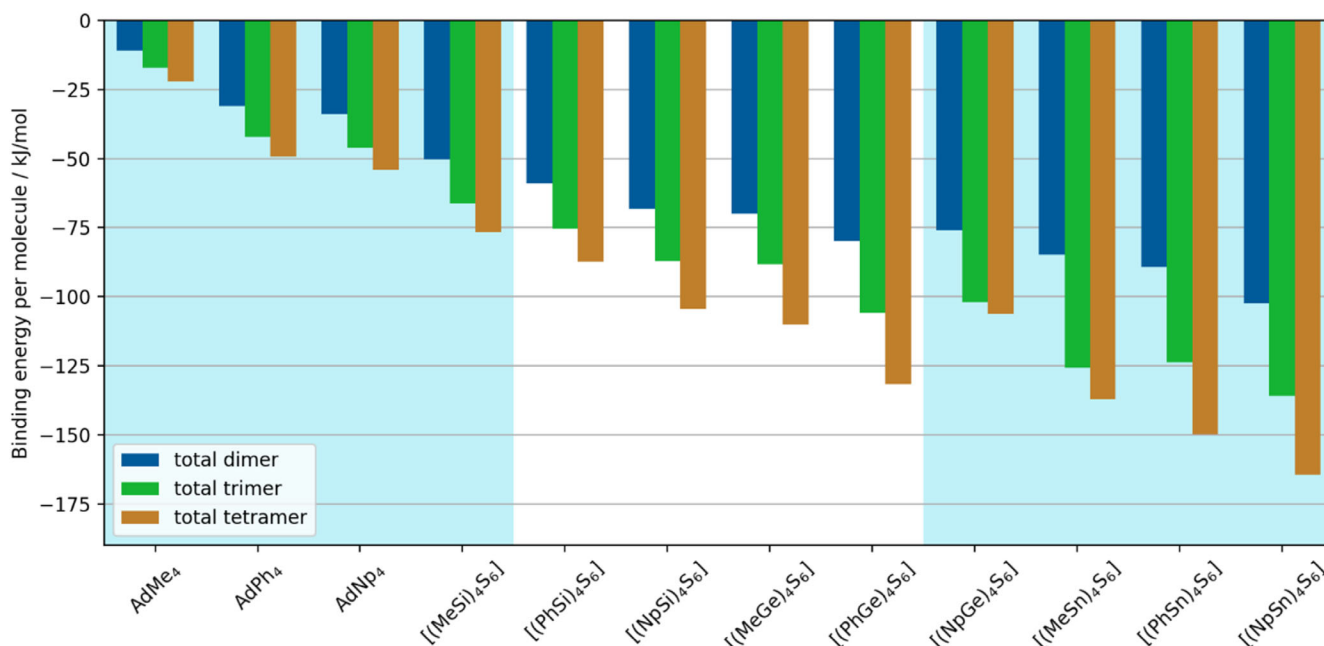


FIGURE 13 Comparison of the total binding energies of the trimer and tetramer systems with the total binding energies of the corresponding dimer systems. For better comparability, the total binding energies were divided by the number of molecules in the system. For all structures, we used the energetic minimum structure as received from CREST, with a subsequent optimization using B3LYP-D3(BJ)/cc-pVDZ level of theory followed by a single point calculation at B3LYP-D3(BJ)/cc-pVTZ level of theory

with the size of the agglomerate (Figure 13). This is to be expected since the main bonding contribution to the binding energy are medium and long-range dispersion interactions that increase with the total size of system.

In summary, the structural properties of larger agglomerates cannot be represented by the lowest energetic minimum structure of the cluster dimer. Here, the inclusion of a variety of cluster dimer conformers seems to be necessary. However, the preferred energetic minimum structures of the cluster dimers provide information as to whether a core–core or substituent–substituent interaction is dominant. Trends regarding the binding energies of the preferred dimer structures appear to be transferable to trimer and tetramer systems.

3 | CONCLUSIONS

We present a systematic analysis of cluster dimers of amorphous materials and single-crystalline cluster materials ($[(RT)_4S_6]$ and AdR_4), for which we gain first insights into the intermolecular interaction within the material. We investigated twelve different chemical compositions in which the adamantane-like core framework and the substituents were varied: $AdMe_4$, $AdPh_4$, $AdNp_4$, $[(MeSi)_4S_6]$, $[(PhSi)_4S_6]$, $[(NpSi)_4S_6]$, $[(MeGe)_4S_6]$, $[(PhGe)_4S_6]$, $[(NpGe)_4S_6]$, $[(MeSn)_4S_6]$, $[(PhSn)_4S_6]$, and $[(NpSn)_4S_6]$. A conformational analysis allowed us to identify typical dimer structures in which orientations displaying small core–core distances are energetically preferred. The type of the global minimum structure is the same for all compounds, namely a staggered structure in which three substituents of one cluster interact with three substituents of the other one.

As the size of the core and the substituents increases, the medium- and long-range dispersion interactions also increase. Separation of the binding energy into contributions from the core and the substituents, respectively, indicates strong core–core interaction for clusters with small substituent or large cores and strong substituent–substituent interactions for clusters with large substituents or small cores. This insight into cluster dimer interactions might serve as a rough indicator of order within the materials, as the isotropic core–core-dominated interactions might lead to a lower tendency for order and the substituent–substituent-dominated interaction to a higher degree of order. Rotational barriers of the substituents and potential energy surfaces of dimer rotations indicate that the substituent rotations might change conformers more easily in the material than rotation of dimer past each other.

The calculation of the nonlinear optical response within the time domain for $AdPh_4$ clusters reveals an overall enhancement of the optical susceptibilities for dimer structures. Further investigations are required to ascertain whether this behavior is a peculiarity of the adamantane clusters or is common to the other systems considered in this work.

The calculation of trimer and tetramer cluster systems shows a consistent trend with the dimers in terms of the minimal core–core distance and binding energies of the global minimum structures. With respect to the orientation of the substituents of the dimers, the structures are not transferable to trimers and tetramers, however, because

of the presence of a variety of orientations within the larger agglomerates. The study thus rationalizes that larger length scales are necessary for a more detailed structural understanding of the material.

The insights gained into the cluster dimer interactions are quite valuable. Fundamental structural features have been determined, the contribution of the binding energy can be used as a rough indicator of the order in the material when core–core or substituent–substituent contributions are dominant, and the nature of the interactions found for different compounds can be compared with relatively small computational effort. This study is therefore the first step toward understanding the structural and energetic properties of adamantane-like materials, which exhibit unique non-linear optical properties.

AUTHOR CONTRIBUTIONS

The manuscript was written through contributions of all authors. All authors have given approval to the final version of the manuscript.

ACKNOWLEDGMENTS

This work was supported by the German Research Foundation within the framework of FOR2824. The authors gratefully acknowledge the computational resources granted by the high performance center of the Justus Liebig University. Open Access funding enabled and organized by Projekt DEAL.

DATA AVAILABILITY STATEMENT

The data that supports the findings of this study are available in the supplementary material of this article.

ORCID

Andreas J. Achazi  <https://orcid.org/0000-0002-3001-875X>

Peter R. Schreiner  <https://orcid.org/0000-0002-3608-5515>

Simone Sanna  <https://orcid.org/0000-0003-4416-0252>

Doreen Mollenhauer  <https://orcid.org/0000-0003-0084-4599>

REFERENCES

- [1] R. Mueller-Mach, G. Mueller, M. R. Krames, H. A. Höpfe, F. Stadler, W. Schnick, T. Juestel, P. Schmidt, *Phys. Status Solidi (A)* **2005**, 202, 1727.
- [2] S. Nakamura, ed. E. F. Schubert, *Present performance of InGaN-based blue/green/yellow LEDs*, Photonics West, **1997**, pp. 26–35.
- [3] F. Kimme, P. Brick, S. Chatterjee, T. Q. Khanh, *Appl. Opt.* **2013**, 52, 8779.
- [4] N. W. Rosemann, J. P. Eußner, E. Dornsiepen, S. Chatterjee, S. Dehnen, *J. Am. Chem. Soc.* **2016**, 138, 16224.
- [5] N. W. Rosemann, J. P. Eußner, A. Beyer, S. W. Koch, K. Volz, S. Dehnen, S. Chatterjee, *Science* **2016**, 352, 1301.
- [6] A. v. Husakou, J. Herrmann, *Phys. Rev. Lett.* **2001**, 87, 203901.
- [7] T. A. Birks, W. J. Wadsworth, P. St. J. Russell, *Opt. Lett.* **2000**, 25, 1415.
- [8] R. R. Alfano, *The Supercontinuum Laser Source*, Springer, New York, New York, NY **2016**.
- [9] H. N. Paulsen, K. M. Hilligse, J. Thøgersen, S. R. Keiding, J. J. Larsen, *Opt. Lett.* **2003**, 28, 1123.
- [10] H. Kano, H. Hamaguchi, *Appl. Phys. Lett.* **2004**, 85, 4298.
- [11] S. Bourquin, A. D. Aguirre, I. Hartl, P. Hsiung, T. H. Ko, J. G. Fujimoto, T. A. Birks, W. J. Wadsworth, U. Bunting, D. Kopf, *Opt. Express* **2003**, 11, 3290.

- [12] M. J. F. Digonnet, *Rare-Earth-Doped Fiber Lasers and Amplifiers, Revised and Expanded*, CRC Press, New York, NY 2001.
- [13] S. Coen, A. H. L. Chau, R. Leonhardt, J. D. Harvey, J. C. Knight, W. J. Wadsworth, P. St. J. Russell, *Opt. Lett.* **2001**, *26*, 1356.
- [14] S. Dehnen, P. R. Schreiner, S. Chatterjee, K. Volz, N. W. Rosemann, W. Pilgrim, D. Mollenhauer, S. Sanna, *ChemPhotoChem* **2021**, *5*, 1033.
- [15] N. W. Rosemann, H. Locke, P. R. Schreiner, S. Chatterjee, *Adv. Opt. Mater.* **2018**, *6*, 1701162.
- [16] E. Dornsiepen, F. Dobener, N. Mengel, O. Lenchuk, C. Dues, S. Sanna, D. Mollenhauer, S. Chatterjee, S. Dehnen, *Adv. Opt. Mater.* **2019**, *7*, 1801793.
- [17] J.-P. Berndt, A. Engel, R. Hrdina, S. Dehnen, P. R. Schreiner, *Organometallics* **2019**, *38*, 329.
- [18] K. Hanau, S. Schwan, M. R. Schäfer, M. J. Müller, C. Dues, N. Rinn, S. Sanna, S. Chatterjee, D. Mollenhauer, S. Dehnen, *Angew. Chem., Int. Ed.* **2021**, *60*, 1176.
- [19] K. Hanau, N. Rinn, S. Dehnen, *Inorg. Chem.* **2020**, *59*, 198.
- [20] K. Hanau, N. Rinn, M. Argentari, S. Dehnen, *Chem. – Eur. J.* **2018**, *24*, 11711.
- [21] E. Dornsiepen, F. Dobener, S. Chatterjee, S. Dehnen, *Angew. Chem., Int. Ed.* **2019**, *58*, 17041.
- [22] A. J. G. Lunt, P. Chater, A. M. Korsunsky, *Sci. Rep.* **2018**, *8*, 1574.
- [23] H. Jo, S. J. Oh, K. M. Ok, *Dalton Trans.* **2017**, *46*, 15628.
- [24] H. Lan, F. Liang, X. Jiang, C. Zhang, H. Yu, Z. Lin, H. Zhang, J. Wang, Y. Wu, *J. Am. Chem. Soc.* **2018**, *140*, 4684.
- [25] S. Grimme, *J. Chem. Theory Comput.* **2019**, *15*, 2847.
- [26] P. Pracht, F. Bohle, S. Grimme, *Phys. Chem. Chem. Phys.* **2020**, *22*, 7169.
- [27] S. Grimme, C. Bannwarth, P. Shushkov, *J. Chem. Theory Comput.* **2017**, *13*, 1989.
- [28] C. Bannwarth, S. Ehlert, S. Grimme, *J. Chem. Theory Comput.* **2019**, *15*, 1652.
- [29] P. Pracht, E. Caldeweyher, S. Ehlert, S. Grimme, *Chem. Rxiv* **2019**, 1-19. <https://doi.org/10.26434/chemrxiv.8326202>
- [30] Turbomole, V7.3 2018, a development of University of Karlsruhe and Forschungszentrum Karlsruhe GmbH, since 2007. <http://www.turbomole.com>.
- [31] F. Furche, R. Ahlrichs, C. Hättig, W. Klopper, M. Sierka, F. Weigend, *WIREs Comput. Mol. Sci.* **2014**, *4*, 91.
- [32] P. A. M. Dirac, *Proc. Royal Soc. (Lond.) A* **1929**, *123*, 714.
- [33] V. Fock, V. V. F. Leningrad, *Z. Phys.* **1930**, *61*, 126.
- [34] J. C. Slater, *Phys. Rev.* **1951**, *81*, 385.
- [35] S. H. Vosko, L. Wilk, M. Nusair, *Can. J. Phys.* **1980**, *58*, 1200.
- [36] A. D. Becke, *Phys. Rev. A* **1988**, *38*, 3098.
- [37] C. Lee, W. Yang, R. G. Parr, *Phys. Rev. B* **1988**, *37*, 785.
- [38] A. D. Becke, *J. Chem. Phys.* **1992**, *96*, 2155.
- [39] K. Eichkorn, F. Weigend, O. Treutler, R. Ahlrichs, *Theor. Chem. Acc. Theory, Comput. Model.* **1997**, *97*, 119.
- [40] K. Eichkorn, O. Treutler, H. Öhm, M. Häser, R. Ahlrichs, *Chem. Phys. Lett.* **1995**, *242*, 652.
- [41] S. Grimme, J. Antony, S. Ehrlich, H. Krieg, *J. Chem. Phys.* **2010**, *132*, 154104.
- [42] S. Grimme, S. Ehrlich, L. Goerigk, *J. Comput. Chem.* **2011**, *32*, 1456.
- [43] S. Grimme, *WIREs Comput. Mol. Sci.* **2011**, *1*, 211.
- [44] T. H. Dunning, *J. Chem. Phys.* **1989**, *90*, 1007.
- [45] R. A. Kendall, T. H. Dunning, R. J. Harrison, *J. Chem. Phys.* **1992**, *96*, 6796.
- [46] B. Metz, H. Stoll, M. Dolg, *J. Chem. Phys.* **2000**, *113*, 2563.
- [47] K. A. Peterson, *J. Chem. Phys.* **2003**, *119*, 11099.
- [48] B. P. Pritchard, D. Altarawy, B. Didier, T. D. Gibson, T. L. Windus, *J. Chem. Inf. Model.* **2019**, *59*, 4814.
- [49] D. Feller, *J. Comput. Chem.* **1996**, *17*, 1571.
- [50] K. L. Schuchardt, B. T. Didier, T. Elsethagen, L. Sun, V. Gurumoorthi, J. Chase, J. Li, T. L. Windus, *J. Chem. Inf. Model.* **2007**, *47*, 1045.
- [51] S. F. Sousa, P. A. Fernandes, M. J. Ramos, *J. Phys. Chem. A* **2007**, *111*, 10439.
- [52] S. Grimme, M. Steinmetz, *Phys. Chem. Chem. Phys.* **2013**, *15*, 16031.
- [53] P. Su, H. Li, *J. Chem. Phys.* **2009**, *131*, 014102.
- [54] L. Pecher, R. Tonner, *WIREs Comput. Mol. Sci.* **2019**, *9*, e1401.
- [55] P. Giannozzi, O. Andreussi, T. Brumme, O. Bunau, M. B. Nardelli, M. Calandra, R. Car, C. Cavazzoni, D. Ceresoli, M. Cococcioni, N. Colonna, I. Carnimeo, A. D. Corso, S. de Gironcoli, P. Delugas, R. A. DiStasio, A. Ferretti, A. Floris, G. Fratesi, G. Fugallo, R. Gebauer, U. Gerstmann, F. Giustino, T. Gorni, J. Jia, M. Kawamura, H.-Y. Ko, A. Kokalj, E. Küçükbenli, M. Lazzeri, M. Marsili, N. Marzari, F. Mauri, N. L. Nguyen, H.-V. Nguyen, A. Otero-de-la-Roza, L. Paulatto, S. Poncé, D. Rocca, R. Sabatini, B. Santra, M. Schlipf, A. P. Seitsonen, A. Smogunov, I. Timrov, T. Thonhauser, P. Umari, N. Vast, X. Wu, S. Baroni, *J. Phys. Condens. Matter* **2017**, *29*, 465901.
- [56] P. Giannozzi, S. Baroni, N. Bonini, M. Calandra, R. Car, C. Cavazzoni, D. Ceresoli, G. L. Chiarotti, M. Cococcioni, I. Dabo, A. Dal Corso, S. de Gironcoli, S. Fabris, G. Fratesi, R. Gebauer, U. Gerstmann, C. Gougoussis, A. Kokalj, M. Lazzeri, L. Martin-Samos, N. Marzari, F. Mauri, R. Mazzarello, S. Paolini, A. Pasquarello, L. Paulatto, C. Sbraccia, S. Scandolo, G. Sclauzero, A. P. Seitsonen, A. Smogunov, P. Umari, R. M. Wentzcovitch, *J. Phys. Condens. Matter* **2009**, *21*, 395502.
- [57] D. Sangalli, A. Ferretti, H. Miranda, C. Attaccalite, I. Marri, E. Cannuccia, P. M. Melo, M. Marsili, F. Paleari, A. Marrazzo, G. Prandini, P. Bonfà, M. O. Atambo, F. Affinito, M. Palumbo, A. Molina Sanchez, C. Hogan, M. Grüning, D. Varsano, A. Marini, *J. Phys. Cond. Matter* **2019**, *31*, 325902.
- [58] A. Dal Corso, *Comp. Mat. Sci.* **2014**, *95*, 337.
- [59] J. P. Perdew, K. Burke, M. Ernzerhof, *Phys. Rev. Lett.* **1996**, *77*, 3865.
- [60] J. P. Perdew, K. Burke, M. Ernzerhof, *Phys. Rev. Lett.* **1997**, *78*, 1396.
- [61] J. P. Perdew, J. A. Chevary, S. H. Vosko, K. A. Jackson, M. R. Pederson, D. J. Singh, C. Fiolhais, *Phys. Rev. B* **1992**, *46*, 6671.
- [62] H. J. Monkhorst, J. D. Pack, *Phys. Rev. B* **1976**, *13*, 5188.
- [63] S. Grimme, *J. Comput. Chem.* **2006**, *27*, 1787.
- [64] I. Souza, J. Íñiguez, D. Vanderbilt, *Phys. Rev. B* **2004**, *69*, 085106.
- [65] C. Attaccalite, M. Grüning, A. Marini, *Phys. Rev. B* **2011**, *84*, 245110.
- [66] C. Attaccalite, M. Grüning, *Phys. Rev. B* **2013**, *88*, 235113.
- [67] P. R. Schreiner, L. V. Chernish, P. A. Gunchenko, E. Y. Tikhonchuk, H. Hausmann, M. Serafin, S. Schlecht, J. E. P. Dahl, R. M. K. Carlson, A. A. Fokin, *Nature* **2011**, *477*, 308.
- [68] H. Ryu, J. Park, H. K. Kim, J. Y. Park, S.-T. Kim, M.-H. Baik, *Organometallics* **2018**, *37*, 3228.

SUPPORTING INFORMATION

Additional supporting information can be found online in the Supporting Information section at the end of this article.

How to cite this article: S. Schwan, A. J. Achazi, F. Ziese, P. R. Schreiner, K. Volz, S. Dehnen, S. Sanna, D. Mollenhauer, *J. Comput. Chem.* **2023**, *44*(7), 843. <https://doi.org/10.1002/jcc.27047>